
Supporting Informaion

Polarity-Dependent Emission from Hydroxyl-Free Carbon Nanodots

Shamsa Kanwal,^{a,b,c} Farukh Mansoor,^b Datao Tu,^{*a} Renfu Li,^a Wei Zheng,^a Shan Lu^a and Xueyuan Chen^{*a}

[a] CAS Key Laboratory of Design and Assembly of Functional Nanostructures, Fujian Key Laboratory of Nanomaterials, and State Key Laboratory of Structural Chemistry, Fujian Institute of Research on the Structure of Matter, Chinese Academy of Sciences, Fuzhou, Fujian 350002, China.

[b] Department of Chemistry, Khwaja Fareed University of Engineering and Information Technology, Abu Dhabi Road Rahim Yar Khan, Pakistan

[c] Fujian Science & Technology Innovation Laboratory for Optoelectronic Information of China, Fuzhou, Fujian 350108, China

E-mail: dttu@fjirsm.ac.cn, xchen@fjirsm.ac.cn

Chemicals and Materials: Ortho-tolunitrile (OTN), meta-tolunitrile (MTN) and para-tolunitrile (PTN) were purchased from TCI. Ethanol (EtOH), chloroform (CHL), dichloromethane (DCM), acetone and cyclohexane (CHX) were bought from Sinopharm Chemical Reagent Co., China. All the chemicals were used without further purification.

Preparation of Carbon nanodots: CNDs were synthesized via a facile solvothermal method by heating a single precursor OTN into teflon-lined autoclaves. After natural cooling, the crude product was washed with excessive amount of CHX followed by centrifugation at 8000 rpm for 6 min to remove unreacted OTN. Control experiments were performed in furnace under air atmosphere by direct heating the OTN in glass vial. Similarly, meta and para derivatives of tolunitrile were also evaluated to prepare CNDs with similar procedures to investigate the prominence of OTN. Very weak PL emission was observed in the case of meta and para-tolunitrile for the samples from the control experiments.

Isolation and purification of CNDs: The as-obtained products from autoclave were mixed and CNDs with distinct surface groups, which were washed with CHX followed by centrifugation at 10000 rpm for 8 min. A solvent

extraction technique was then used to separate and purify the produced CNDs. Subsequently, CNDs with different surface groups were intelligently separated via silica column chromatography, where silica gel with mesh size of 70-230 and solvents like CHX, CHL and EtOH were used. For a quick and smooth flow of solvent, the column was equipped with a constant flow of N₂ pressure (0.2 MPa). Order of elution with respect to nature of solvents was followed, where non-polar solvent like cyclo-hexane (CHX) was mixed with different ratios of less polar solvent like chloroform (CHL) to separate non-polar CNDs named as NP-CND1 (blue emission), NP-CND2 (orange emission) and NP-CND3 (blue emission) as shown in Table S1. Subsequently, gradual rise in polarity by utilizing ethanol (EtOH) with different ratios of CHL to obtain P-CND1 (green emissions), P-CND2 (white emission) and P-CND3 (yellow emission), respectively. Generally, CNDs of different polarities were collected as 500-800 mL fraction in particular solvent system combination in 40 mL glass vials. These fractions were rechecked under UV lamp and concentrated on the rotary evaporator.

Instrumentation for Structural and Optical Characterizations: UV-visible characterization was conducted on Perkin-Elmer Lambda 365. Fourier transform infrared (FTIR) spectra were recorded in KBr discs on a Magna 750 FTIR spectrometer. Excitation and emission scans were performed on FLS980 spectrometer (Edinburgh Instrument) equipped with both continuous xenon (450 W) and pulsed flash lamps. The absolute quantum yield (QY) of CNDs was measured at RT by mounting a barium-sulfate coated integrating sphere (150 mm in diameter, Edinburgh) as the sample chamber on FLS920 spectrometer having input as well as output port of the sphere located at 90° from each other in the plane of the spectrometer. Closed cycle cryostat (10–350 K, DE202, Advanced Research Systems) was used for low-temperature measurements. A standard tungsten lamp was used to correct the optical response of the instrument. All the spectral data were recorded at RT and corrected for the spectral response of both the spectrometer and the integrating sphere. PL photographs of the samples were taken using a canon digital camera without using any filter. Decay studies were conducted using a 397-nm picosecond pulsed laser on FLS980.

Both the low- and high-resolution transmission electron micrograph (TEM) measurements were performed by using a JEOL-2010 TEM equipped with the energy dispersive X-ray spectrum operated at 200 kV. Atomic force microscopy (AFM) images were recorded with Bruker dimension ICON, after preparing samples on mica. X-ray photoemission spectroscopy (XPS) spectra were measured on a SPECS Sage HR 100 spectrometer (Thermo fisher

ESCALAB250xi) using a non-monochromatised Mg-K α radiation of 1253.6 eV and 250 W (monochromatised Al-K α radiation of 1486.6 eV and 300 W), in an ultrahigh vacuum chamber at a pressure of 1×10^{-9} mbar. For each analysis, an aqueous solution (~ 3 mg/mL) of the material was deposited on a gold thin film (silicon). Calibration was done using the 3d $_{5/2}$ line of Ag(C $_{1s}$). Survey and high-resolution spectra were collected with pass energy of 30 (100) and 15 (20) eV and 0.5 (1) and 0.15 (0.1) eV/step, respectively. CasaXPS 2.3.17 PR1.1 and Avantage (Thermo Fisher Scientific) softwares were used for data processing and fitting. Curve fittings of the C1s, N1s and O1s spectra were realized using a Gaussian-Lorentzian peak shape after performing a Shirley (smart) background correction, to finally obtain the relative percentage of all types of bonds inside the analyzed sample.

Table S1. Solvent system of different polarities used for separation of CNDs through silica column chromatography. The estimated solvent run to separate each fraction of CNDs and their corresponding PL photographs under 365 nm irradiation are also displayed.

Sample	Solvent system Volume ratio (mL)	Estimated solvent run (mL)	Photographs under 365 nm irradiation
NP-CND1	Cyclohexane: Chloroform 35:65	600	
NP-CND2	Cyclohexane: Chloroform 33:67	500	
NP-CND3	Cyclohexane: Chloroform 20:80	750	
P-CND1	Chloroform: Ethanol 99.14:0.86	700	
P-CND2	Chloroform: Ethanol 98.8:1.2	750	
P-CND3	Chloroform: Ethanol 97.5:2.5	750	

Table S2. FTIR data analysis and peak assignments for NP-CNDs and P-CNDs. Functional group assignment indicates that the surface of NP-CNDs mainly contains C=O, while the surface of P-CNDs is N-rich.

Wavenumber (cm ⁻¹)	Functional Group assignment	NP-CNDs	P-CNDs
1020-1100	C-O-C	√	√
1260	-C-O	√ ^[a]	X
1388	-C-N=	√	√
1544	-C=C	√	√
1646	-C=N	√	√
1738	-C=O	√ ^[a]	√
2850-2960	-C-H alkyl group	√	√
3440-3470	-N-H or -H-N-H	x	√

[a] maximum in NP-CND2

Table S3. XPS analysis of NP-CNDs and P-CNDs with different percentages of O1s, N1s and O1s/N1s ratios. It can be observed that NP-CND2 contains the maximum content of O1s. Besides, O1s/N1s ratios for P-CNDs were determined to be smaller than that for NP-CNDs.

Sample	O1s (%)	N1s (%)	O1s/N1s (%)
NP-CND1	18.92	1.29	14.67
NP-CND2	21.75	1.28	16.92
NP-CND3	15.02	1.22	12.31
P-CND1	12.08	2.74	4.4
P-CND2	6.51	3.35	1.94
P-CND3	8.35	11.78	0.708

Table S4. Comparison of bonding types through high-resolution XPS data analysis of C1s and N1s spectra for NP-CNDs and P-CNDs. More C=C/C=O as well as C-O-C groups and less amino-NH group were detected in NP-CNDs than in P-CNDs.

Sample	C=C/C-C	C-O-C	C=O	Amino-NH
NP-CND1	71.16	4.34	1.39	x
NP-CND2	79.24	7.82	4.12	x
NP-CND3	72.92	5.17	1.14	x
P-CND1	70.17	0.97	1.11	2.53
P-CND2	67.39	0.88	1.07	4.31
P-CND3	68.05	0.81	1.01	5.46

Table S5. Effective PL lifetimes (T_{eff}) of NP-CNDs and P-CNDs upon excitation with a 397-nm picosecond pulsed laser. T_{eff} was calculated by

$$\tau_{\text{eff}} = \frac{1}{I_{\text{max}}} \int_0^{\infty} I(t) dt$$

where $I(t)$ denotes the PL intensity as a function of time t , and I_{max} is the maximum PL intensity.

Sample	$\tau_{(1)\text{eff}}$ (ns)	$\tau_{(2)\text{eff}}$ (ns)	$T_{(\text{avg})\text{eff}}$ (ns)
NP-CND1	0.3 (47.34%)	3.2 (53.66%)	1.3
NP-CND2	0.41 (48.55%)	3.1 (51.45%)	1.5
NP-CND3	0.83 (48.55%)	4.5 (51.55%)	2.2
P-CND1	0.70 (62.66%)	6.19 (37.34%)	3.1
P-CND2	0.94 (34.57%)	5.3 (65.43%)	3.8
P-CND3	2.2 (27.73%)	5.45 (72.27%)	4.5

Table S6. PL parameters of NP-CNDs and P-CNDs and their corresponding absolute PLQYs. The absolute PLQY of each sample was measured three times independently under identical conditions to yield the mean value and relative standard deviation. It can be observed that NP-CNDs exhibit higher PLQY than P-CNDs.

Sample	Emission/excitation (nm)	PLQY (%)
NP-CND1	435/340	30.8 ± 0.2
NP-CND2	578/340	23.4 ± 0.7
NP-CND3	437/350	55.9 ± 0.5
P-CND1	497/350	20.7 ± 0.2
P-CND2	593/360	4.5 ± 0.5
P-CND3	555/340	2.1 ± 0.3

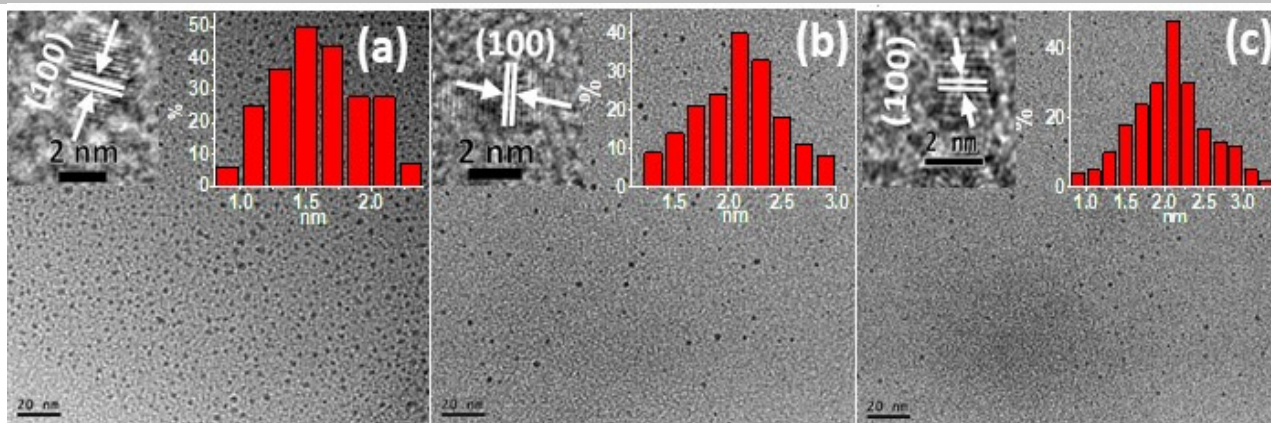


Figure S1. TEM images of (a) P-CND1, (b) P-CND2, and (c) P-CND3. Insets show corresponding HRTEM images and histograms of size distribution obtained by calculating 200 particles from TEM images. These results indicate that there is no noticeable variation in size and crystal spacing of P-CNDs.

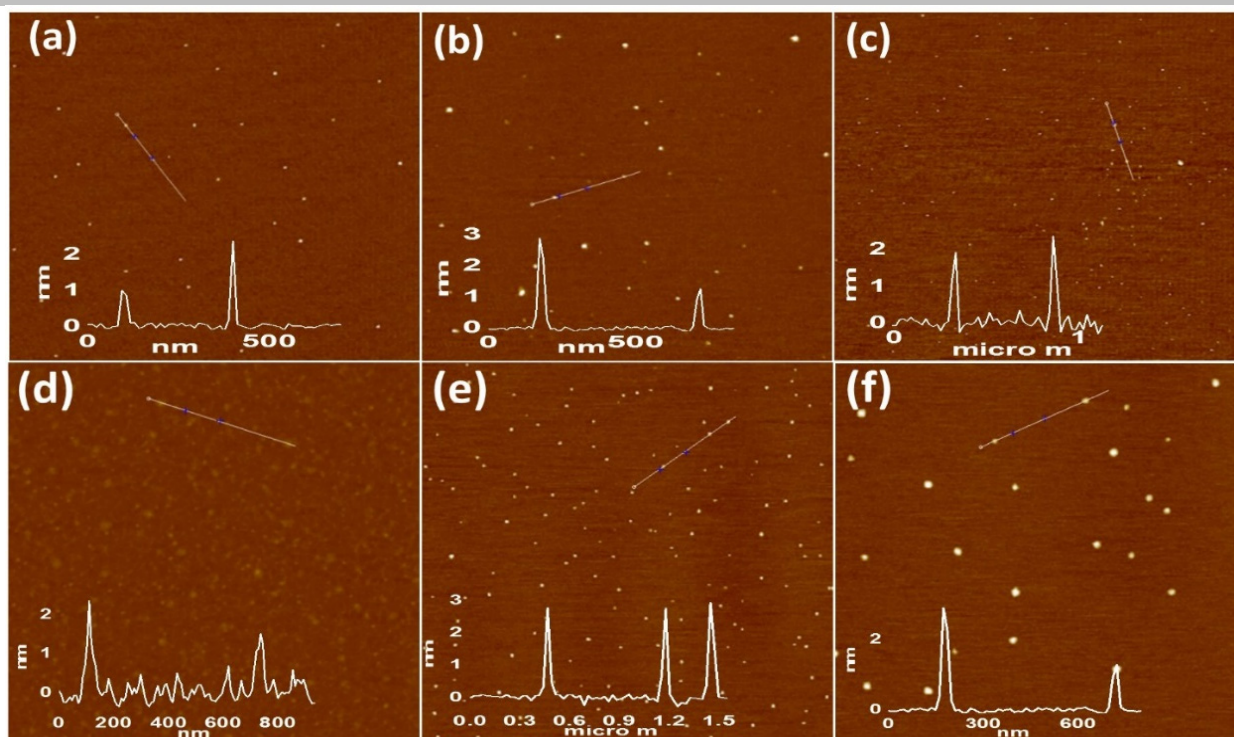


Figure S2. Tapping mode AFM images of (a) NP-CND1, (b) NP-CND2, (c) NP-CND3; and (d) P-CND1, (e) P-CND2, (f) P-CND3 on a (5.0 x 5.0 mm) mica substrate (insert: height profiles). These images show no noticeable variation of height profiles and morphology of NP-CNDs and P-CNDs.

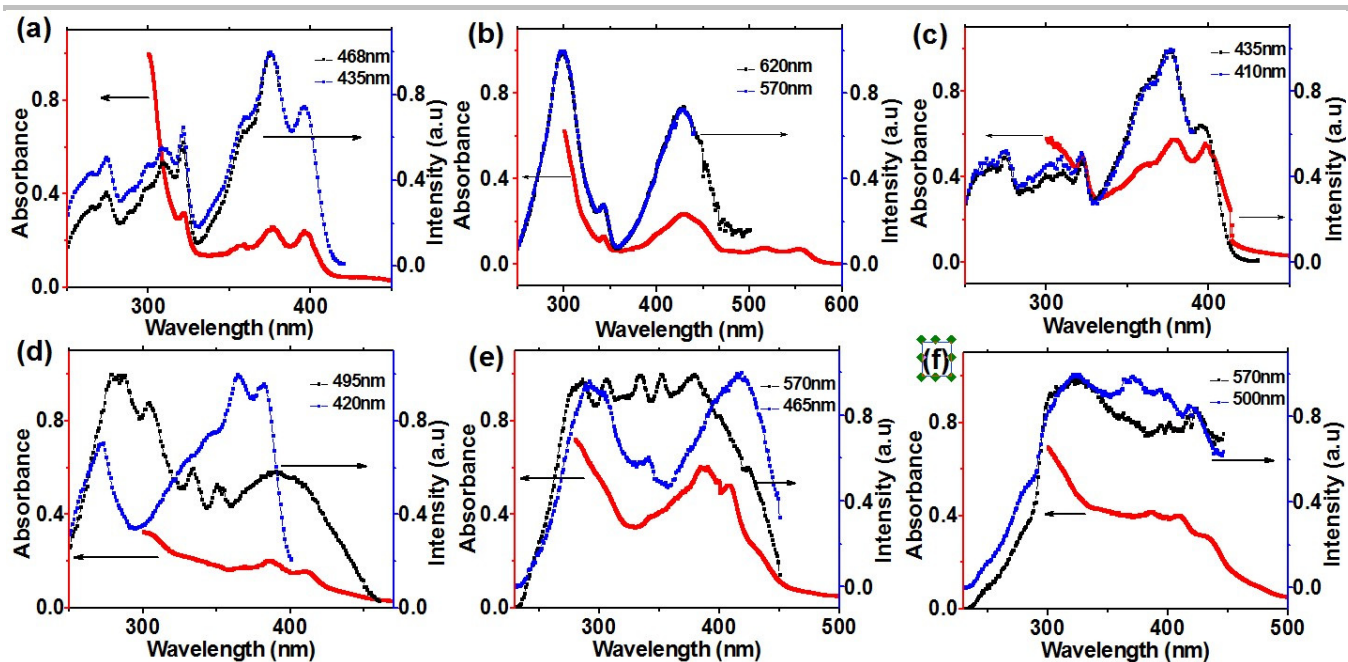


Figure S3. Comparison of UV-vis absorbance (red) and PL excitation spectra (blue, black) for (a) NP-CND1, (b) NP-CND2 and (c) NP-CND3. Comparison of UV-vis absorbance (red) and PL excitation spectra (blue, black) for (d) P-CND1, (e) P-CND2 and (f) P-CND3. PL excitation spectra were recorded at various emission wavelengths mentioned in each set. Absorption and excitation peaks of the (a-c) NP-CNDs exhibited overlapping effect, while non-overlapping of absorption and excitation peaks (d-f) were observed for P-CNDs.

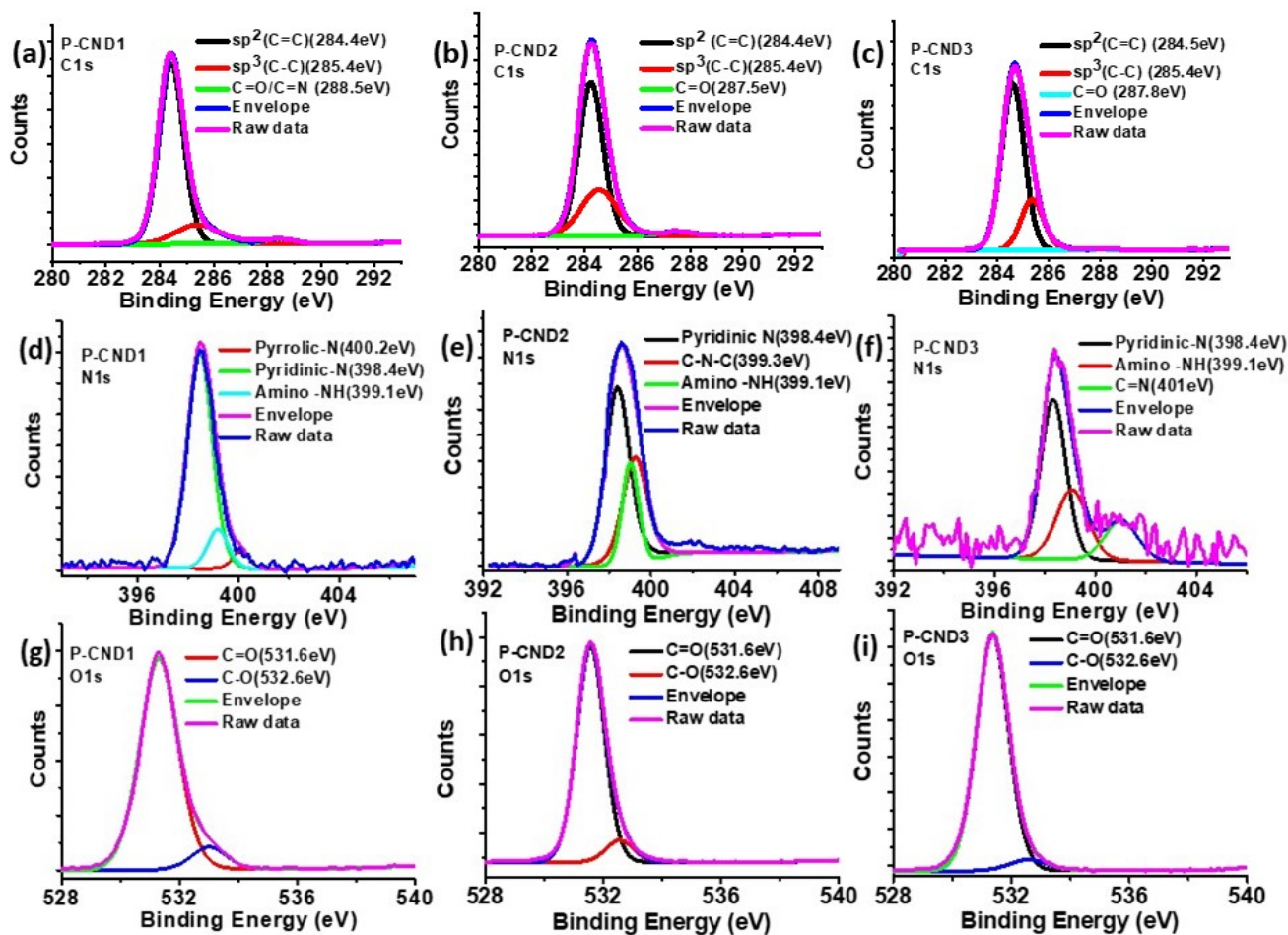


Figure S4. High-resolution XPS (a-c) C1s, (d-f) N1s, and (g-i) O1s spectra of P-CND1, P-CND2 and P-CND3, respectively. Quenched C=O and C-O peaks can be observed in the case of C1s and O1s spectra. Amino-NH peak appears at 399.1 eV in N1s spectra of P-CNDs. Peaks are assigned according to the literature.^[1]

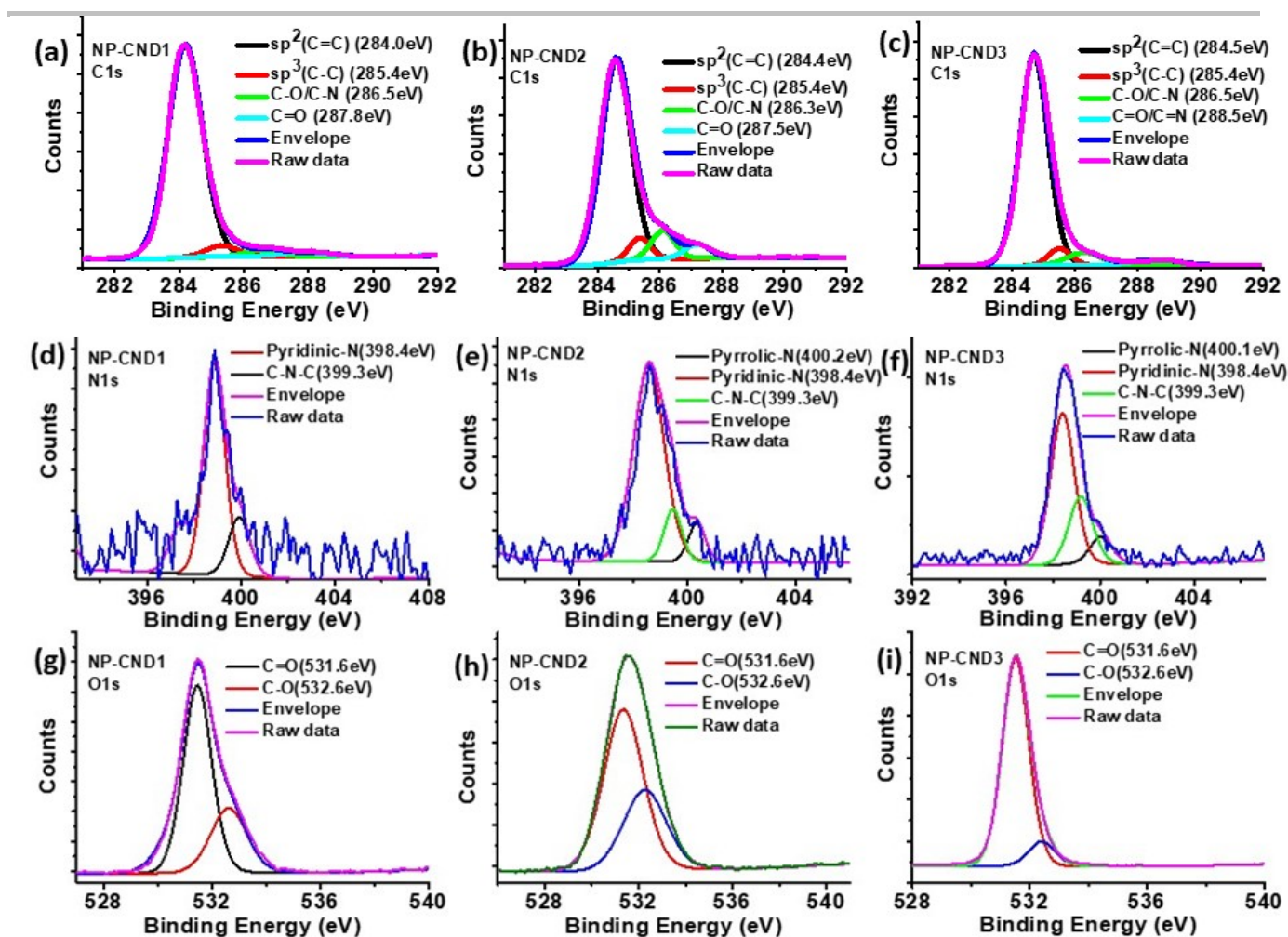


Figure S5. High-resolution XPS of (a-c) C1s, (d-f) N1s, and (g-i) O1s spectra for NP-CND1, NP-CND2 and NP-CND3, respectively. C1s and O1s spectra indicate high content of C=O and C-O and low content of amino-NH in NP-CNDs. The absence of amino-NH peaks in the case of N1s spectra (d-f) confirms the non-polar nature of NP-CNDs. Peaks are assigned according to the literature.^[1]

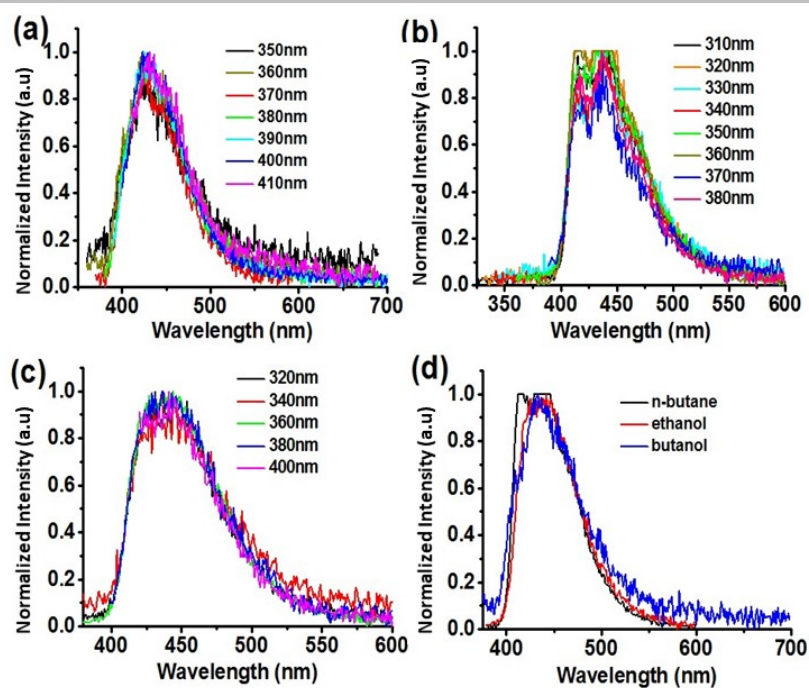


Figure S6. PL emission spectra of NP-CND3 in (a) n-butane, (b) n-butanol and (c) EtOH upon excitation at different wavelengths. (d) Comparison of PL emission spectra of NP-CND3 in n-butane, n-butanol and EtOH upon excitation at 320 nm. No obvious change in PL peak position was observed for NP-CND3 in polar and non-polar solvents.

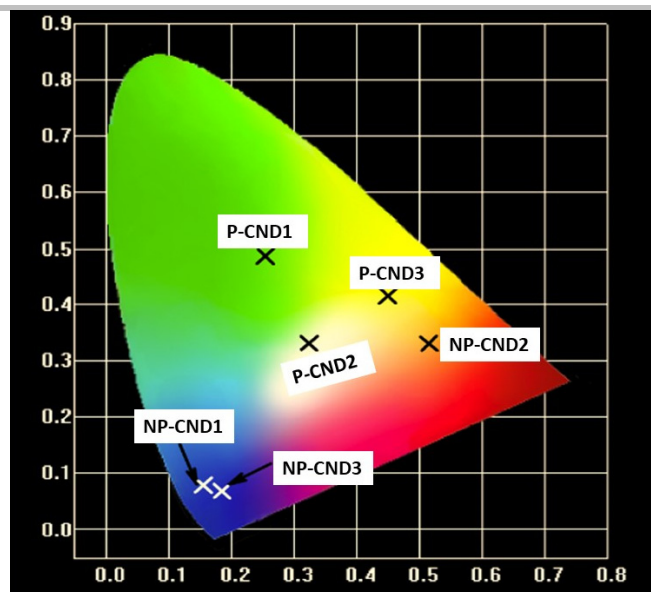


Figure S7. 1931 CIE chromaticity chart displaying coordinates of a set of NP-CNDs and P-CNDs. White emission can be achieved for P-CND2 with coordinates at ($x=0.332$, $y=0.336$).

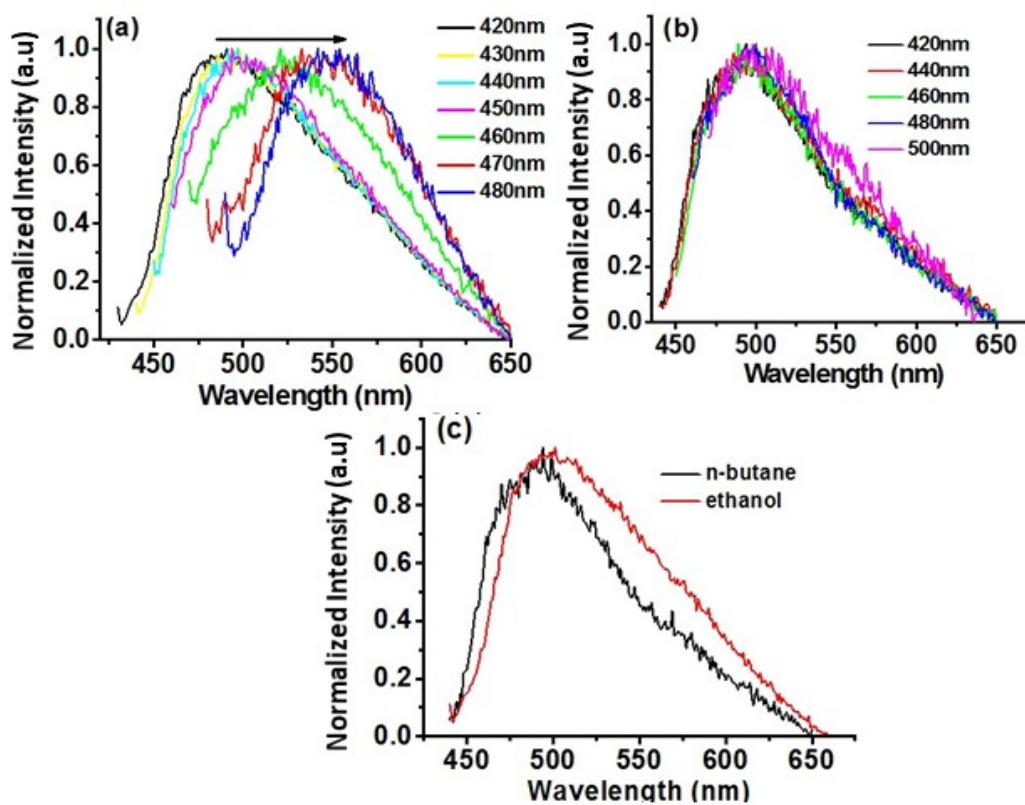


Figure S8. PL emission spectra of P-CND1 in (a) EtOH and (b) n-butane upon excitation at different wavelengths. (c) Comparison of PL emission spectra of P-CND1 in EtOH and n-butane upon excitation at 420 nm. PL peak position red shifted greatly in polar solvent (EtOH). However, no change in the PL peak position was observed in non-polar solvent (n-butane) with increasing the excitation wavelength.

References

- [1] a) S. Qu, D. Zhou, D. Li, W. Ji, P. Jing, D. Han, L. Liu, H. Zeng, D. Shen, *Adv. Mater.* **2016**, *28*, 3516-3521;
b) K. Jiang, S. Sun, L. Zhang, Y. Lu, A. Wu, C. Cai, H. Lin, *Angew. Chem. Int. Ed.* **2015**, *54*, 5360-5363;
Angew. Chem. **2015**, *127*, 5450-5453; c) H. Ding, S. -B. Yu, J.-S. Wei, H. -M. Xiong, *ACS Nano* **2015**, *10*,
484-491; d) H. Nie, M. Li, Q. Li, S. Liang, Y. Tan, L. Sheng, W. Shi, S. X. -A. Zhang, *Chem. Mater.* **2014**,
26, 3104-3112.